

1

The Electronic Structure of Solids

Uwe Bovensiepen, Silke Biermann, and Luca Perfetti

The discussion of dynamics at interfaces is based on the motion of ion cores and electronic excitations that are mostly optically driven. Hence, the electronic structure is of fundamental importance here. In solids such as molecular or ionic crystals, the valence electron distribution is not considerably distorted from the respective isolated atoms, ions, or molecules. Hence, their cohesion is entirely given by the classical potential energy of negligibly deformed electron distributions of bare particles, and van der Waals or Coulomb interactions are responsible for the formation of solid materials. This ceases to be so in metals and covalent crystals because the valence electron distribution plays the decisive role in bonding the constituents to a solid. In turn, the valence electron distribution can be considerably modified from the isolated atom or ion. A general description of solids must, therefore, consider the electronic structure in the first place. Furthermore, the dynamical processes discussed in this book are mostly optically excited or electron mediated.

This chapter introduces the basic concepts widely used in the description of the electronic structure in solid materials. In Section 1.1, we present the description of the nearly free electron approximation that is motivated by optical excitations of a solid following the Drude model. We introduce the Fermi sphere and the dispersion of electronic bands in momentum space. In Section 1.2, the influence of the periodic potential in a crystal is considered, which leads to the description of the electronic band structure by Bloch's theory for delocalized states. There is a considerable variety of materials that is not described by band theory, which originates from electron–electron interaction. In Section 1.3, we introduce Mott insulators that manifest deviations from the band picture. In Section 1.4, we introduce established concepts to describe the electronic structure of materials with strong electron correlations and give examples.

1.1

Single-Electron Approximation

Although a solid contains about 10^{23} electrons/cm³, for a number of materials (but not for all) it is sufficient to neglect the explicit interaction among these particles. In this one-electron approximation, the energy of individual electrons is renormalized to account for the electron–electron interaction, which simplifies the description enormously. These electrons in the material are then termed quasi-particles.

1.1.1

The Drude Model of the Free Electron Gas

We start by considering propagation of electrons in a metal. Such dynamical processes have been essential for Drude’s theory of electrical conductivity in metals [1] and will be discussed in detail in Chapter 5. Here, we introduce the concept briefly in order to motivate the description of the electronic structure in solids.

Drude applied the kinetic theory of gases to a metal that is represented by a gas of electrons occupying the interstitial region between the ion cores. Without an electric field \mathbf{E} , the current density $\mathbf{j} = -nev$ averages to zero because the electrons have no preferential direction to move at velocity \mathbf{v} in between two collisions with scattering centers (which Drude imagined to be the ion cores); here, n represents the electron density and e the elementary charge. In the presence of an electric field, a net current density $\mathbf{j} = -nev$ develops because during the time interval $\tau = 1/\Gamma$ between two collisions the electron is accelerated in a preferential direction to $\mathbf{v} = -e\mathbf{E}\tau/m$. The electrical DC conductivity σ_0 is hence proportional to the time τ between two scattering events.

$$\mathbf{j} = \sigma_0\mathbf{E}; \quad \sigma_0 = \frac{ne^2\tau}{m}. \quad (1.1)$$

Here, m is the electron mass. To estimate the order of magnitude of τ , the measured DC conductivity is taken, for example, for Cu at a temperature $T = 77$ K and one finds $\tau \approx 2.1 \times 10^{-13}$ s or 210 fs being well in the femtosecond regime.

If the electric field is time dependent, the result can be generalized for a frequency ω to

$$\mathbf{j}(\omega) = \sigma(\omega)\mathbf{E}(\omega); \quad \sigma(\omega) = \frac{\sigma_0}{1 - i\omega\tau}. \quad (1.2)$$

Using the wave equation for the electric field $-\nabla^2\mathbf{E} = \omega^2/c^2\varepsilon(\omega)\mathbf{E}$, the complex dielectric function $\varepsilon(\omega)$ is introduced.

$$\varepsilon(\omega) = 1 + \frac{4\pi i\sigma(\omega)}{\omega}. \quad (1.3)$$

With ω_p being the plasma frequency, the dielectric constant according to Drude’s theory reads after linearization in $1/\tau$

$$\varepsilon(\omega) = 1 - \frac{\omega_p^2}{\omega^2} + i \frac{\omega_p^2}{\omega^3} \frac{1}{\tau}; \quad \omega_p^2 = \frac{4\pi n e^2}{m}. \quad (1.4)$$

Considering the reflectivity $R = ((1-n)^2 + k^2)/((1+n)^2 + k^2)$ with $n = \text{Re}\sqrt{\varepsilon}$ and $k = \text{Im}\sqrt{\varepsilon}$, an electromagnetic wave cannot penetrate into the bulk of a metal for $\omega < \omega_p$ because it is reflected. For large frequencies $\omega > \omega_p$, it does propagate in a metal. The absorption is proportional to the scattering rate $\Gamma = 1/\tau$ and $1/\omega^3$. The latter is usually referred to as the free carrier response, which will become clear further below. Please note that Drude's considerations are very fundamental throughout this book and will be used with emphasis on different aspects in Chapter 5.

The absorption is determined by $\text{Im } \varepsilon = (4\pi/\omega)\text{Re } \sigma$ and can be deduced from a measurement of the reflectivity using, for example, the Kramers–Kronig relations. Figure 1.1 shows the experimental results for alkali metals. At low frequency, the pronounced increase in absorption according to the free carrier response (Eq. (1.4)) is readily visible. At higher frequency, the behavior exhibits particular signatures that are characteristic for the respective material. For an understanding of the absorption spectrum in the visible and the ultraviolet spectral range, we consider next the electronic structure in the single (or independent) electron approximation.

A considerable improvement of Drude's theory was achieved by including the Pauli principle and Sommerfeld implemented the Fermi–Dirac velocity distribution

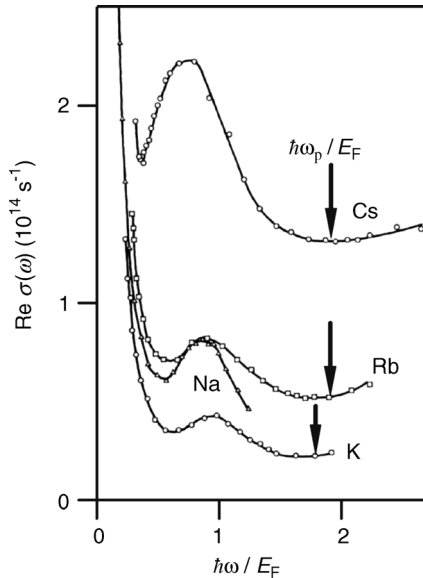


Figure 1.1 Optical absorption spectra of alkali metals (adapted from Ref. [2]). At low frequency the Drude-like increase in absorption originating from the free carrier response is

clearly seen. At higher frequency, specific absorption peaks due to interband excitation are found. Arrows indicate the plasma frequency ω_p in units of E_F/\hbar for Cs, Rb, and K.

of electrons leading to the free electron gas. In this description, the electrons do not interact with each other, which is usually termed the independent electron approximation. Electrons populate single-particle states beginning from the smallest energy. The states with different wave vectors $k = (k_x, k_y, k_z)$ in a particular three-dimensional volume $V = L_x \cdot L_y \cdot L_z$ are defined by $k_i = 2\pi n_i / L_i$ with $i = x, y, z$ and n_i being integer numbers. Hence, the electrons populate the states up to a maximum energy E_F , which defines the Fermi sphere in k -space. The momentum $\hbar k_F$ is termed the Fermi momentum and $E_F = \hbar^2 k_F^2 / 2m$ is the Fermi energy.

1.1.2

The Electronic Band Structure: Metals, Insulators, and Semiconductors

Before the interband transitions observed in Figure 1.1 can be understood, the periodic arrangement of ion cores in a crystal lattice must be considered.

Indeed, both the ionic potential and the electronic density follow the periodicity of the solid. It is convenient to consider this periodicity in the description of the electronic structure. For free electrons, it is reasonable to consider that the electron wave vector components k_x, k_y, k_z attain absolute values between zero and infinity in a continuous and uniquely defined manner. For electrons in a periodic potential, however, an electronic wave can experience Bragg reflection. This adds the wave vector of the respective periodicity in the crystal, which is described by a reciprocal lattice vector with an absolute value $G = 2\pi/a$ with a being the lattice constant responsible for the periodic potential, to the electron wave vector. Therefore, the electron wave vector in a periodic crystal is defined by $2\pi/\lambda \pm n \cdot 2\pi/a$, with n being an integer number. Consequently, the electron wave vector in a periodic potential is no longer uniquely defined. It is helpful to transfer a wave vector by the appropriate number of Bragg reflections to its smallest absolute value within the interval $-\pi/a < k < \pi/a$. Taking the lattice symmetries and the respective variation of the lattice constant a along different high-symmetry directions into account, the smallest volume in the three-dimensional wave vector space that contains all available back-folded wave vectors is defined as the first Brillouin zone. In Figure 1.2, the electron band is plotted in the first Brillouin zone along the direction from Γ to N in the bcc lattice of sodium.

In the independent electron approximation, the effects of electron–electron interactions are entirely accounted for by an effective potential $U(\mathbf{r})$, which also respects this periodicity. Within this framework, the electronic wave functions are determined by the time-independent Schrödinger equation with the periodic potential $U(\mathbf{r})$. Vibrations of the ion cores and deviations from a perfect periodicity due to defects, for example, are neglected at this stage. In the case of the nearly free electron approximation, the periodic potential is included as a weak perturbation of the free electron gas.

It turns out that the nearly free electron approximation is quite reasonable for simple metals with predominant s, p -like valence electrons. Prominent examples are the alkali metals and aluminum. To assign the peak in the optical absorption spectrum of alkalis observed in Figure 1.1 at $\hbar\omega/E_F \approx 1$, the occurrence of

band gaps at the boundary of the Brillouin zone is important. Free electron wave functions, which resemble traveling waves $\psi_k \propto \exp i\mathbf{k}\mathbf{r}$, are found in the center of the Brillouin zone in the vicinity of the band bottom. The crystal periodicity offers the possibility for Bragg reflection of electron waves in the vicinity of the Brillouin zone boundary. The respective wave functions are a superposition of waves traveling in opposite directions. The different phase of the resulting standing waves leads to accumulation of electron probability density either in the vicinity of the ion cores, where the potential is deep, or in the interstitial region where the potential is shallow and rather flat. The different energy of these two situations results in an energy gap close to the Brillouin zone boundary. The gap size is determined by the periodic perturbation of the free electron gas potential.

It is a well-known exercise of introductory textbooks to calculate the interband transition threshold for alkali metals in the nearly free electron approximation [3]. The resulting threshold is $0.64 \hbar\omega/E_F$, which agrees well with the noticeable rise in absorption at energies above $0.64 \hbar\omega/E_F$ reported in Figure 1.1. This energy represents a threshold because for higher optical energies a combination of an occupied and unoccupied state can be found that can be excited by a direct optical transition. Such a direct transition proceeds vertically in the electron dispersion diagram as illustrated in Figure 1.2 and zero momentum change occurs concomitantly with the transition. Energy and momentum are also conserved for indirect excitations as depicted also in Figure 1.2 for an excitation where the initial and final

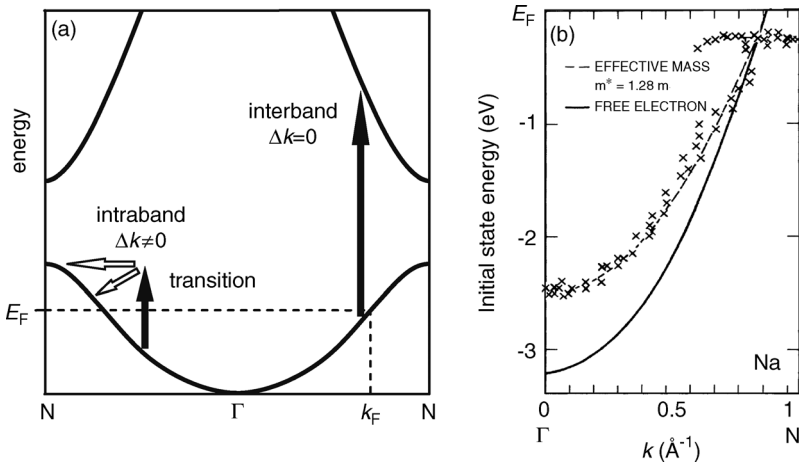


Figure 1.2 Typical dispersion of electron wave functions with wave vector in the nearly free electron approximation. In (b) experimental results from angle-resolved photoelectron spectroscopy as a function of photon energy from Ref. [4] are shown by crosses. For an introduction to this technique, we refer to Chapter 3. The solid line represents a calculation

on the nearly free electron approximations; the dashed line fits a modified effective electron mass to the data. In (a) direct interband and indirect intraband transitions are indicated. The latter require a compensation of the momentum change to maintain energy and momentum conservation.

states belong to the same band. Here, a vertical transition is not possible in case of perfect crystal periodicity. However, a defect or a lattice distortion can absorb the required momentum change Δk and facilitate the transition in an elastic or inelastic manner. Further details are beyond the present introduction and can be found in Chapter 5.

By including the d -orbitals into electronic structure calculations, optical interband transitions from d to s, p states add significant excitation pathways and are responsible for the characteristic optical reflection spectrum of noble metals and hence their color.

To describe the electric conductivity, the population of the bands is essential. A material for which the valence electrons fill the uppermost populated band completely will be an insulator because an applied electric field will not cause electrical current to flow. If a band is partially filled, the electric field can move the carriers and the material is a metal. Considering the Pauli principle, a crystal can be an insulator only if the number of valence electrons in the primitive unit cell is an even integer. Otherwise, it is expected to be metallic. As will be discussed in the forthcoming section, this expectation is in general not always met, albeit it holds for many simple materials. Insulators and semiconductors are distinguished although both have a completely occupied valence band because thermal excitations in semiconductors facilitate a considerable electrical conductivity, which increases further with increasing temperature.¹⁾ In insulators, the gap is in general large enough to suppress thermally induced conductivity. However, under particular conditions, insulators can conduct an electric current, for example, after optical excitation or by ion propagation.

1.2

From Bloch Theory to Band Structure Calculations

1.2.1

Bloch Theory

Bloch's theorem teaches us that the eigenstates of a quantum particle in a periodic potential are of the form $\Psi_{n\mathbf{k}}(\mathbf{r}) = u_{n\mathbf{k}}(\mathbf{r}) \exp(i\mathbf{k}\mathbf{r})$, where $u_{n\mathbf{k}}(\mathbf{r} + \mathbf{R}) = u_{n\mathbf{k}}(\mathbf{r})$ for all \mathbf{R} of the Bravais lattice. The wave vector \mathbf{k} lies in the first Brillouin zone and the band index n is an additional quantum number. The corresponding probability of finding the particle at a given point in the solid is thus a periodic function with the periodicity of the lattice: the electron is delocalized over the whole solid.

The eigenstates of a system of N noninteracting electrons are Slater determinants of Bloch states. The same remains true if interactions are taken into consideration but approximated by a static mean field, such as the electrostatic Hartree potential or a more refined effective potential resulting, for example, from a description by density

1) The temperature dependence of electrical conductivity facilitates a clear distinction of metals and semiconductors. While in semiconductors the conductivity can increase with temperature, it generally decreases in metals because of the increased electron-phonon scattering.

functional theory. Indeed, in the absence of two-particle terms in the Hamiltonian, the latter can be expressed as a sum of N (identical) one-particle Hamiltonians. This “independent electron approximation” thus leads necessarily to a band picture of the solid. In the ground state of the N -electron system, the resulting one-particle Bloch states corresponding to the N lowest lying one-particle (band) energies are filled. If the occupied state at the highest energy lies within a band, the system is metallic in this picture. Conversely, if a fully filled conduction band and an empty valence band are separated by a gap, we are dealing with an insulator.

1.2.2

The Tight Binding Approach to the Solid

An elementary approach to the band structure of a solid, complementary to the nearly free electron approach, is the tight-binding approximation. It describes the solid as a collection of atoms, weakly perturbed by their neighbors. The deviation from atomic behavior originates from the so-called overlap integrals, matrix elements of electronic wave functions centered on neighboring atoms: $\gamma_{ij}(\mathbf{R}) = -\int d\mathbf{r} \psi_i^*(\mathbf{r}) \Delta U(\mathbf{r}) \psi_j^*(\mathbf{r})$, where the Hamiltonian $H = H_{\text{at}} + \Delta U(\mathbf{r})$ is separated into an atomic part and a correction. The latter is responsible for the coupling, that is, the delocalization of electrons over the solid. Mathematically speaking, the tight binding approach consists in searching for the Bloch functions as solutions of Schrödinger’s equation in the periodic potential of the solid in the form of linear

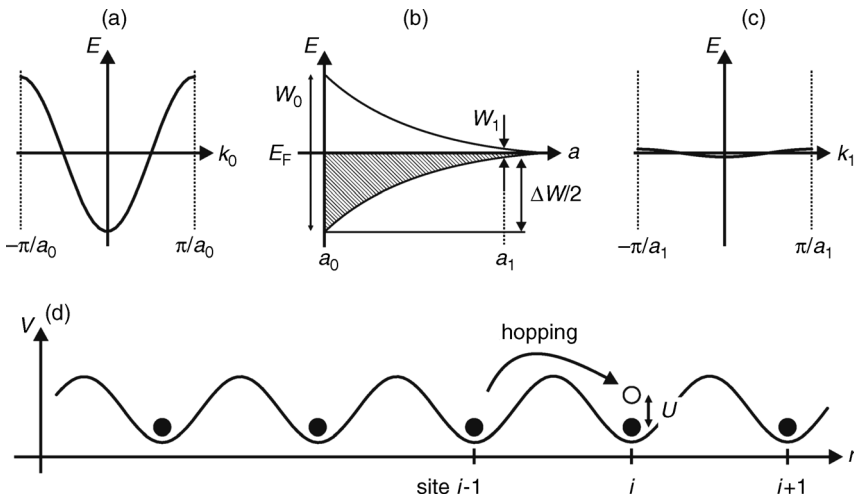


Figure 1.3 Schematic representation of the competition between kinetic energy or band width W and Coulomb repulsion U . (b) depicts the reduction in band width with increasing lattice constant a . In (c) and

(a) the effect of band width on the dispersion of the single-electron band structure is depicted. In (d) the energy U required to populate two electronic states at one localized site is illustrated.

combinations of atomic orbitals. It is clear from this picture that quite extended orbitals lead to large overlap integrals and thus large band width, whereas core or semicore states give rise to dispersionless bands of negligible band width; see Figure 1.3a–c for illustration.

1.2.3

Band Structure Calculations

As seen above, once the independent electron approximation has been chosen, the electronic states are of Bloch form, and the corresponding eigenvalues are known as the band structure of the solid. To calculate it quantitatively, a choice for the effective interaction potential has to be made. The most natural choice that one may think of is the electrostatic potential created by a charge distribution corresponding to the electronic density, the so-called Hartree potential. This is, however, not the approximation chosen for most quantitative calculations nowadays. Indeed, the “Kohn–Sham potential” of density functional theory often yields band structures in better agreement with experimental observations. Density functional theory is an exact theoretical framework that associates with the interacting electron system an auxiliary noninteracting system of the same density in an effective potential: these two systems have the same ground-state properties. Strictly speaking, the theoretical framework does not attribute any physical meaning to the corresponding eigenvalues; nevertheless, they often represent a not too bad approximation to the electronic band structure observed in experiments. We do not enter here in the vast literature on the subject, but the reader interested in the relation of the Kohn–Sham gap and an electronic excitation gap of an insulator may be directed to the work of Perdew [5]. An additional difficulty consists in the fact that while the existence of the effective Kohn–Sham potential is established by the fundamental theorems of density functional theory, its explicit form is unknown, and in practical calculations further approximations have to be made. The most popular among them is the so-called local density approximation (LDA), which adds to the Hartree term an exchange–correlation contribution based on the homogeneous electron gas.

1.3

Beyond the Band Picture

The importance of band theory for the development of modern solid-state physics can hardly be overestimated. In combination with theories proposing appropriate effective potentials approximating the electronic Coulomb interactions by one-particle potentials, band theory gave a framework to the first attempts of *quantitative* descriptions and predictions of electronic properties of solids. Nevertheless, one did not have to wait for the more and more complex materials synthesized in modern materials science to find examples where band theory fails.

1.3.1

Mott's Hydrogen Solid

A simple argument by Mott [6] already shows the limits of the band description. Consider a collection of atoms with a single valence electron and a single orbital, for example, hydrogen, and let us forget for the moment their tendency to molecule formation. Arranging the atoms in a periodic structure with one atom per unit cell and a lattice constant a of the order of Å results – according to Bloch's theorem – in a half-filled band and thus in a metallic state; see Figure 1.3. The physical mechanism behind the band formation is the kinetic energy gain associated with the delocalization of the electrons. Now consider the following *Gedankenexperiment* (see Figure 1.3a–c): let us increase the lattice constant to artificially large values a_1 , so as to decrease the kinetic energy gain and in particular to make it smaller than the price of the Coulomb interaction U that we have to pay when two electrons occupy the same atom, as illustrated in Figure 1.3d. In this situation, hopping becomes unfavorable, and the ground state consists of electrons being localized on their respective atoms. The system is just reduced to a collection of independent atoms. In other words, in this “atomic limit” the ground state is *not* the Slater determinant of Bloch states postulated by Bloch's theorem. It is the competition with the Coulomb interaction associated with double occupancies that destroys the Bloch state. In fact, in this situation it is more appropriate to think in terms of real space rather than in k -space. To first approximation, we can entirely neglect the kinetic energy and write the effective Hamiltonian for the Coulomb interactions:

$$H_{\text{int}} = \sum_i U n_{i\uparrow} n_{i\downarrow} \quad (1.5)$$

Here, $n_{i\sigma}$ denotes the occupation number operators corresponding to an electron in the s -orbital on site i with spin σ ; they commute with the Hamiltonian and are good quantum numbers. The Hamiltonian is thus diagonal in the eigenbasis of these operators, and the eigenstates can be labeled simply by these atomic occupation numbers. We are, therefore, naturally led to a real space picture. This is in contrast to the kinetic energy part of the Hamiltonian

$$H_{\text{kin}} = \sum_{ij\sigma} t_{i\sigma} c_{j\sigma}^\dagger c_{i\sigma}, \quad (1.6)$$

which is diagonal in momentum space. Indeed, Fourier transformation of the creation and annihilation operators for an electron at site i and with spin σ , $c_{i\sigma}^\dagger$, and $c_{j\sigma}$ according to

$$c_{k\sigma}^\dagger = \sum_{j\sigma} \exp(ikR_j) c_{j\sigma}^\dagger \quad (1.7)$$

$$c_{k\sigma} = \sum_{j\sigma} \exp(ikR_j) c_{j\sigma} \quad (1.8)$$

diagonalizes the Hamiltonian

$$H_{\text{kin}} = \sum_{k\sigma} \varepsilon_k c_{k\sigma}^\dagger c_{k\sigma} \quad (1.9)$$

Here, the R_r denotes the lattice sites and the k -vectors are the crystal momenta as in Bloch's theorem.

Despite its simplicity, the above example illustrates the physical mechanisms at work in systems that require a description beyond one-particle approaches. Indeed, in between the two limits – the band picture of noninteracting Bloch electrons and the atomic limit of localized electrons – the situation becomes much more complicated. The physics is determined by the competition of kinetic energy W and Coulomb interaction U , and the general N -particle state is not just a Slater determinant of one-particle states. The Hamiltonian is diagonal neither in real nor in Fourier space.

Before entering into a more detailed theoretical modeling of the resulting N -particle physics, we will discuss some examples of real materials where correlated electron physics enters into play.

1.3.2

Mott Insulators in Nature

At the early stage of quantum mechanics, Verwey reported that many transition metal oxides with partially filled d -electron bands were poor conductors or even insulators [7]. This finding is in sharp contrast with the prediction of band theory, thus questioning the basic hypothesis of the independent electron approximation. Indeed, in these compounds the Coulomb repulsion U between two electrons occupying a d -orbital could become larger than the energy gain due to the electronic delocalization. When this is the case, a half-filled electronic system gains energy by a complete localization of the charges into a Mott insulating phase. In reality, the orbital degeneracy of the d -electron systems can oversimplify the description in terms of a single-conduction band [8]. This orbital degeneracy is an unavoidable source of complicated behavior, as the colossal magnetoresistance observed in the manganites. In many materials, the physics of low-energy excitation is also determined by the overlap of the d -orbitals of the transition metals with the p -band of ligand atoms. If the p -band is situated close to the Fermi energy, the character of the minimum charge excitation gap corresponds to the transition from a state with fully occupied p -band to a state with an extra electron in the d -band and a p -like hole. The existence of such charge transfer insulators has been experimentally demonstrated by resonant photoemission spectra of NiO [9]. Zaanen *et al.* classified the transition metal oxides on the basis of their charge gap energy and on-site Coulomb repulsion U [10]. It follows that lighter and heavier transition metals tend to generate a charge transfer and Mott insulator, respectively. However, it should be noticed that a clear separation between charge transfer insulators and Mott insulators is not possible in the presence of significant hybridization of the p - d orbitals. As an example, the oxygen p -orbitals of high-temperature superconductors are strongly hybridized with $d_{x^2-y^2}$ orbitals, leading to a single band crossing the Fermi level. As a consequence, an effective

Hubbard model with a single band is often considered to account for the physics of the high-temperature superconductors.

The phase diagram of Mott insulators can be experimentally determined by varying the temperature, by electronic filling, or by applying external perturbations. For example, the hydrostatic pressure reduces the interatomic distances and changes the crystal field. These effects increase the conducting band width and affect the orbital degeneracy. Alternatively, the same process can be obtained by varying the original stoichiometry through chemical substitution of isoelectronic elements. The phase diagram for $V_{1-x}Cr_xO_3$ shows that pressure and chemical substitution induce comparable effects on the physical properties [11]. As shown by Figure 1.4, a first-order transition connects the paramagnetic insulating phase to the paramagnetic metallic phase. At low temperature, the material enters an antiferromagnetic phase that extends to relatively high pressure. The transition from the paramagnetic insulator to the metal has for a long time been attributed to a gradual increase in the

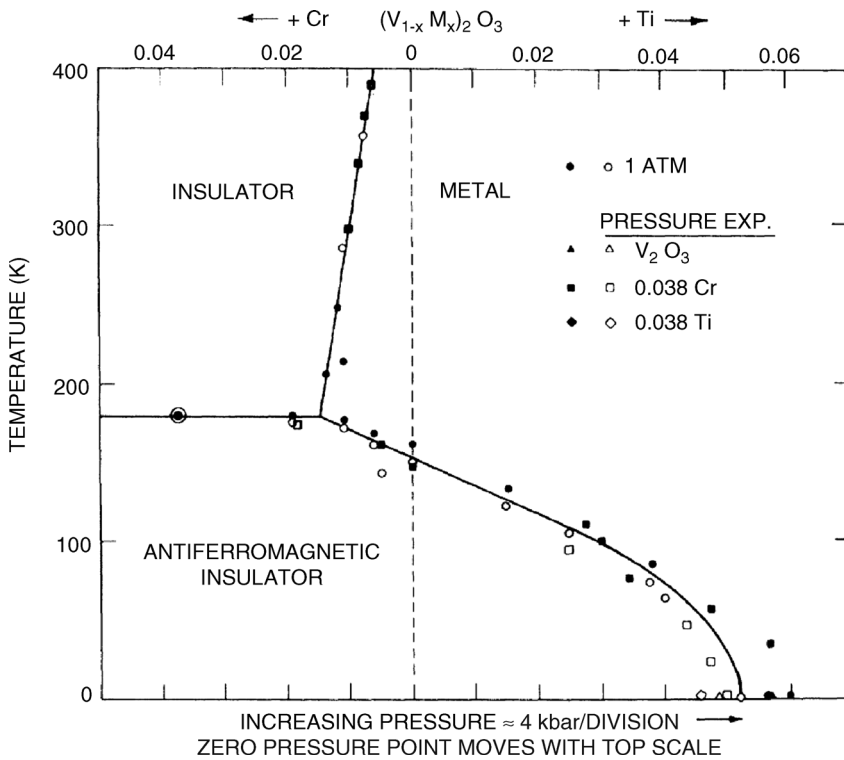


Figure 1.4 Phase diagram for the metal insulator transition in $(V_{1-x}M_x)_2O_3$ as a function of temperature (left axis) and pressure (bottom axis). Square symbols are for $M = Cr$ and $x = 0.038$. The electronic substitution of V with Cr or Ti impurities induces a lattice distortion

acting as an effective pressure. The equivalence is shown by the circular symbols, which have been obtained at ambient pressure and varying the concentration of Cr or Ti (top axis); reprinted with permission from Ref. [11]. Copyright (1971) by the American Physical Society.

electronic band width of an occupied d -orbital with respect to the electronic correlation. This process is known as a band width-controlled transition and can be qualitatively explained by the Hubbard-like models of the electronic Hamiltonian. However, it is currently understood that the metal–insulator transition of $V_{1-x}Cr_xO_3$ is possible only because of a larger – and correlation-enhanced – crystal field of the insulating phase [12]. The crystal field removes some of the orbital degeneracy of the d -shell. In the case of a cubic symmetry, the crystal field splits the d -states in a threefold degenerate t_{2g} level and a doubly degenerate e_g level. The stretching of the oxygen octahedra around the transition metal atom may further reduce the point group symmetry of the crystal field. It appears that an external pressure induces a structural distortion that may modify the orbital energies even more than the electronic band width. Indeed, more examples have been recently analyzed, where the orbital degrees of freedom play a crucial role in metal–insulator transitions. We do not enter here the involved description of the multiorbital Mott transition. Instead, we discuss the metal–insulator transition in the model compound $1T-TaSe_2$ that has been investigated in the framework of a one-band Hubbard model. Theory predicts a large transfer of spectral weight from the Fermi level to a localized feature that is termed a lower Hubbard band. An unavoidable coupling to the lattice degrees of freedom results in a first-order characterization of this transition. As shown in Figure 1.5, the evolution of electronic states across a band width-controlled transition of $1T-TaSe_2$ is in reasonable agreement with theoretical expectations [13].

Another, qualitatively different method of inducing the transition from a Mott insulator to a metallic phase is obtained by changing the band filling. This is experimentally realized by doping the material with elements having different valence. Even small deviations from an integer occupation of the orbitals generates dramatic effects on the electronic properties. Figure 1.6 shows the optical conductivity spectra of $La_{1-x}Sr_xTiO_{3+y}$ and $Y_{1-x}Ca_xTiO_3$ [15]. The hole doping of such titanates is achieved by varying the concentration x of the alkaline earth element. It

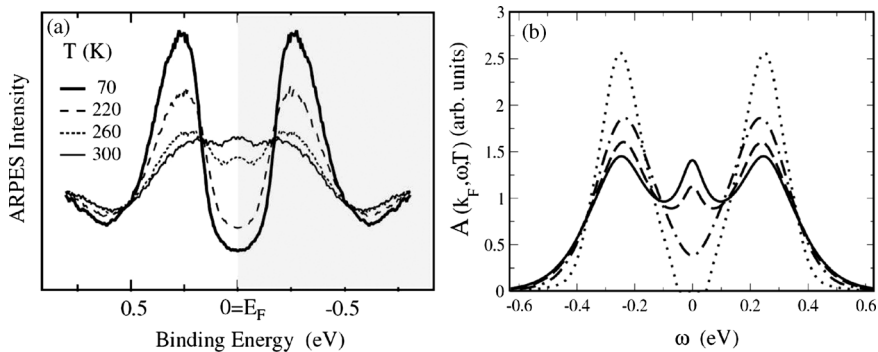


Figure 1.5 (a) Temperature-dependent ARPES data for $1T-TaSe_2$ that represent the spectral function of the system. The curves have been obtained by symmetrization of the raw spectra around the Fermi level. (b) Temperature-dependent spectral function of

the half-filled Hubbard model calculated within DMFT for the temperatures corresponding to the experiment; reprinted with permission from Ref. [13]. Copyright (2003) by the American Physical Society.

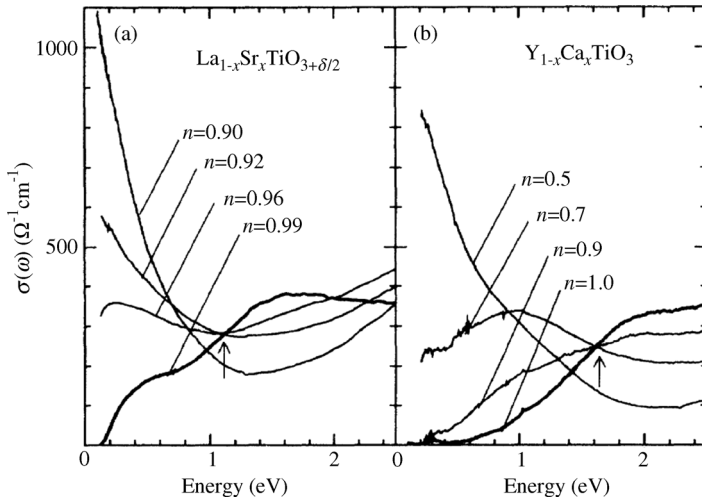


Figure 1.6 Real part of the optical conductivity determined from optical spectra for two types of carrier-doped perovskite titanates with change of the band filling n ; reprinted with permission from Ref. [15]. Copyright (1995) by the American Physical Society.

follows a filling-controlled metal–insulator transition that causes an abrupt increase for a photon energy of 0.1 eV and above, as can be seen in Figure 1.6 with decreasing n . This finding is consistent with the occurrence of an insulating ground state in such a material. Upon doping $\text{La}_{1-x}\text{Sr}_x\text{TiO}_{3+y}$ with few percentages of electrons per unit cell, the transfer of spectral weight takes place on an energy scale 10 times larger than the energy of the gap. This redistribution of the spectral properties over a wide interval of energy is a hallmark of strong electronic interactions. Furthermore, the low-energy excitations appearing below the gap value are largely “incoherent.” In the DC limit, the electronic mean free path predicted by the Drude model becomes comparable or even smaller than the lattice constant. Such anomalous scattering rate makes the electron dynamics of such materials very different from the usual Drude behavior, discussed in Section 1.1, and precludes any description in terms of nearly independent particles.

Finally, the photoexcitation of electron–hole pairs is a novel and interesting approach to perturb the Mott insulating phase. Notice that photoexcitation is very different from filling or band width control. In most cases, the charge fluctuations generated by the laser field thermalize within few femtoseconds, leading to a quasi-stationary distribution of the electronic excitations. Under this condition, the average filling of the electronic states is not changed with respect to the equilibrium state. A first idea of the photoexcitation can be obtained by considering the ratio U/W as constant. At sufficiently large excited carrier density, the Mott insulator becomes unstable and the correlation gap collapses. This process can be modeled by a large increase in the electronic temperature while leaving the lattice degrees of freedom unchanged. The outcome of photoexcitation is a pseudogap-like phase corresponding to an incoherent metal with reduced density of the electronic states close to the

Fermi level. The presence of a quasi-particle peak in such a pseudogap-like state has been detected in $1T\text{-TaS}_2$ and requires further experimental and theoretical investigations [16].

1.4

Electronic Structure of Correlated Materials

In the following sections, we provide an introduction to electronic states of materials in which effects of electronic correlation are essential. Their description is involved and real materials are further complicated by dimensionality effects and crystal fields, and the emergence of ordered states, which makes these systems very interesting. We concentrate on essential concepts and provide illustrative examples that we consider helpful for an introduction.

1.4.1

The Hubbard Model

The above theoretical considerations and the given experimental results indicate the importance of the interplay of delocalization due to the kinetic energy gain and the localization due to Coulomb interactions. The most simple model that takes this competition into account was formulated by John Hubbard, Martin Gutzwiller, and Junjiro Kanamori:

$$H = \sum_{ij\sigma} t c_{i\sigma}^\dagger c_{j\sigma} + \sum_i U n_{i\uparrow} n_{i\downarrow} \quad (1.10)$$

It describes the competition between the energy gain due to delocalization of the electrons and the Coulomb interaction. Indeed, the expectation value of the double occupation $\langle n_{i\uparrow} n_{i\downarrow} \rangle$ is finite in the delocalized state, leading to an interaction energy that can – for narrow band systems – compete with the kinetic energy contribution.

The microscopic justification of the Hubbard model relies on the introduction of a localized basis set, spanning the low-energy Hilbert space of the one-particle part of the Hamiltonian, and on the calculation of the effective Coulomb interaction acting on those degrees of freedom. To simplify the discussion, let us assume for the moment that we are dealing with a system where the low-energy band states can be derived from a single atomic orbital, replicated to all atomic sites R , $\chi_R(r)$ is then a Wannier function of the system, and in this case, the Fourier transform of the Bloch eigenstate $\chi_k(r)$. When writing the full crystal Hamiltonian on the basis of the atomic orbitals, among the matrix elements of the Coulomb interaction

$$U(R, R') = \int dr dr' |\chi_R(r)|^2 |\chi_{R'}(r')|^2 v_{\text{screened}}(r, r') \quad (1.11)$$

the on-site ($R = R'$) term dominates because it describes the high Coulomb energy required to create doubly occupied atomic sites.

For an account of the microscopic derivation, we refer the reader to the original papers [17]. In one dimension, the model (1.10) is exactly solvable and exhibits the effects special to this case, which are in particular Tomonaga–Luttinger behavior and spin–charge separation. Here, we focus on the basic physical effects that this model displays in higher dimensions. Apart from the one-dimensional case, this model allows for yet another limit where the exact solution can be investigated, which is the case of infinite lattice coordination. Indeed, in this case the dynamical mean field theory described below gives the exact solution.

The phase diagram for this case is given in Figure 1.7. At sufficiently low temperature, the phase diagram of the Hubbard model displays a metal–insulator transition as a function of the interaction, as expected from the qualitative discussion of the atomic and band limits above. The transition – except at zero temperature – is of first order, displaying a pronounced coexistence region, where both an insulating and a metallic phase can be stabilized. The sharp metal–insulator transition ends at a high-temperature critical point, above which a crossover between a phase that is referred to as “bad metal” and insulating behavior can be found.

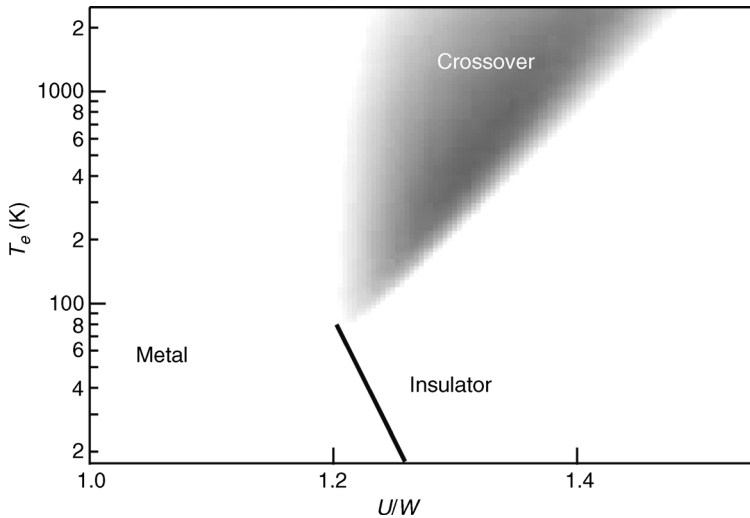


Figure 1.7 Phase diagram of the half-filled one-band Hubbard model within dynamical mean field theory. The physics of the model depends on two parameters: the ratio of the Coulomb interaction U over the band width W in eV and the temperature T . A paramagnetic metal-to-insulator transition from a Fermi liquid phase at weak interactions (small U) to a Mott insulator at large interactions (large U) is observed at intermediate temperatures.

The transition in this framework is first order with a coexistence region plotted in gray scale where both the metallic and the insulating phases can be stabilized. At low temperatures, depending on the lattice geometry, magnetically ordered phases are more favorable. At high temperatures, the metal–insulator transition is replaced by a crossover from a bad metal to a semiconducting or insulating regime.

Formally, the exact solution holds for infinite dimensions, meaning for a lattice model where each site has an infinity of nearest neighbors. The above scenario is believed to be a reasonable approximation also in the three dimensions in the regime not too close to the metal–insulator transition.

The spectral properties of the Hubbard model have been calculated by means of dynamical mean field theory (DMFT). As shown in Figure 1.5, the electronic spectrum of the insulating phase displays two pronounced peaks separated by the on-site repulsion U . In the atomic limit, this term corresponds to the expected amount of energy that is necessary to add an electron to the system. Figure 1.5 shows that the Hubbard peaks at finite binding energy are present even in the metallic phase. Therefore, the electronic excitations still have considerable projection on localized states. On the other hand, a third peak emerges at the Fermi level. This feature has the character of a quasi-particle band with weak energy dispersion. Therefore, the electronic excitations also have a finite projection on delocalized states, but with an effective mass that is largely renormalized by the Coulomb interaction. This duality between the localized and itinerant character of the electronic excitations is probably the most surprising and interesting outcome of the model.

It is, therefore, more than an academic exercise to describe how the above solution can be obtained. This is the subject of the following section, devoted to DMFT.

1.4.2

Dynamical Mean Field Theory

The basic idea of DMFT is to replace a lattice problem (or in the realistic case, the solid) by an effective local system, coupled to a bath and subject to a self-consistency condition, in analogy to conventional Weiss mean field theory in statistical mechanics. Contrary to the latter, however, the intervening mean field is energy dependent, hence the notion of a dynamical MFT.

Let us illustrate the method with the example of the single-band Hubbard model, as defined by the Hamiltonian

$$H = \sum_{ij\sigma} t_{ij} \left(c_{i\sigma}^\dagger c_{j\sigma} + c_{j\sigma}^\dagger c_{i\sigma} \right) + \sum_i U n_{i\uparrow} n_{i\downarrow}. \quad (1.12)$$

Dynamical mean field theory associates with this Hamiltonian an auxiliary *local* problem, defined by the *Anderson impurity* Hamiltonian

$$H = \sum_l \left(\varepsilon_l d_{l\sigma}^\dagger d_{l\sigma} + V_l c_{0\sigma}^\dagger d_{l\sigma} + V_l^* d_{l\sigma}^\dagger c_{0\sigma} \right) + U n_{0\uparrow} n_{0\downarrow} \quad (1.13)$$

The latter describes the physics of one of the original lattice sites (labeled here as 0), coupled to a bath (operators d , d^\dagger) through a hybridization V_l . The bath has an infinity of degrees of freedom labeled by l , at energies ε_l . This model was originally introduced by P. W. Anderson for describing an impurity in a host material [18]. Within dynamical mean field theory, it is reinterpreted in the following way. The impurity

site 0 represents an arbitrary site of the original lattice, and the bath plays the role of the mean field representation of the lattice. In contrast to the original ideas of Anderson who wrote an impurity model in order to describe a physical impurity in a (given) host material, the impurity within the DMFT context is representative of a correlated orbital at a given site of a translationally invariant solid. The bath is thus a quantity that has to be determined self-consistently in order to maintain the translational invariance of the lattice.

In practice, the computational task consists in calculating the local Green's function $G_{\sigma}^{\text{imp}} = -\langle \hat{T} c_{L\sigma} c_0^{\dagger} \rangle$ of the above local impurity model. Here, the brackets denote the thermodynamical average taken with the density matrix of the Anderson impurity model Hamiltonian (1.13), and \hat{T} is the time-ordering operator. For the explicit calculation of the Green's function, a variety of techniques, ranging from Monte Carlo simulations to approximate schemes, are available. As in standard mean field theory, there is a second step related to restoration of the translational invariance of the original model. Imposing that all equivalent sites behave in this same way yields a self-consistency condition that eventually determines the parameters of the Anderson impurity model. Mathematically speaking, one imposes the local Green's function G of the solid to equal the impurity Green's function G^{imp} . To this effect, the self-energy of the impurity model $\Sigma_{\text{imp}} = \mathcal{G}_0^{-1} - G^{-1}$ is calculated and used as an approximation to the full self-energy of the lattice. Thus,

$$G(i\omega_n) = \sum_{\mathbf{k}} [i\omega_n + \mu - H_0(\mathbf{k}) - \Sigma^{\text{imp}}(i\omega_n)]^{-1}. \quad (1.14)$$

In practice, this set of equations is solved iteratively, starting from a guess for the bath parameters ε_l , V_l , solving the impurity model, inserting the corresponding self-energy into the self-consistency equation (1.14), recalculating the bath from Dyson's equation, using the result to update the impurity model, and so on.

1.4.3

Electronic Structure Calculations

We have discussed in the preceding sections two strategies of theoretical modeling: the first one, a band structure approach, is appealing in that it treats the solid from *first principles* (i.e., without any adjustable parameters). The electronic Coulomb interactions, however, are included within static mean field theory. We have mentioned above why this strategy fails for solids with localized electrons. The second strategy, shown in the example of the Hubbard model, consists of studying the interplay of localized and delocalized behavior within the most simple models that incorporate the competition between kinetic energy and Coulomb interactions. While very successful for assessing the basic mechanisms, for example, of correlation-driven metal-insulator transitions, this approach obviously takes a very simplistic view on the chemistry of a compound, namely, by including only one band and an effective hopping between sites. It provides no information about the effect of multiorbital Coulomb correlations, hybridization between different bands, the influence of crystal

field splittings, and so on. To address a given compound, an attractive way to arrive at a material-specific description is to include hopping, hybridization, and crystal field in the band structure calculations, and then to use the resulting one-particle Hamiltonian as a starting point for a *multiorbital* Hubbard-type Hamiltonian that can be treated within many-body techniques. This strategy is realized in the recent combination of density functional theory with dynamical mean field theory, the so-called “LDA + DMFT” scheme.

The basic idea of constructing a local model for the purpose of calculating a local self-energy as an approximation to the full many-body self-energy of the system carries directly over from the model context to the case of a real solid. The most basic version of the combined “LDA + DMFT” scheme [19, 20] can be viewed as a DMFT solution of a multiorbital Hubbard model, where the parameters are calculated from DFT-LDA. The impurity represents the correlated orbitals of a type of atoms in the solid, and the self-consistency condition attributes the same self-energy to all equivalent correlated atoms – up to rotations in orbital space.

From a conceptual point of view, LDA + DMFT in its general framework can be viewed as an approximation to a functional of both the density and the spectral density of correlated orbitals, as formulated within spectral density functional theory [25].

As an illustration of DMFT, we discuss calculations of correlated metals and Mott insulators for the series of d^1 perovskite compounds SrVO_3 , CaVO_3 , LaTiO_3 , and YTiO_3 . These compounds, while isoelectronic and (nearly) isostructural, display a radically different behavior. The vanadates are moderately correlated metals with a mass enhancement of about a factor of 2, while the titanates are insulating. LDA + DMFT calculations for these compounds were able to unravel the underlying mechanism [26]: a tiny difference in the orbital occupations, which are induced by GdFeO_3 -type distortions already at the band structure level, is amplified by the electronic Coulomb interactions and leads to an orbitally polarized insulating behavior. For YTiO_3 , for example, the orbital polarization results in an effective single-band model; this reduction of the degeneracy suppresses the kinetic energy, and even moderate Coulomb interactions fully localize the system.

1.4.4

Ordered States

We briefly mentioned in the previous section that metal insulator transitions can also arise from the symmetry breaking of spin, orbital, or lattice degrees of freedom. In the case of symmetry breaking, the insulating phase can be reached through the vanishing carrier number with no need for mass enhancement. It was pointed out by Landau that it is not possible to analytically deform a state of one phase into the state of a phase having different symmetry [28, 29]. Typically, the more symmetric phase is on the high-temperature side of the accessible states and the less symmetric phase on the low-temperature side. This happens because the Hamiltonian of a system usually exhibits all the possible symmetries of the system, whereas the low-energy states lack some of these symmetries. At low temperatures, the system tends to be confined to the low-energy states. At higher temperatures, thermal fluctuations increase the

probability to find states with higher energy. The system explores a larger portion of phase space, thus favoring a more symmetric solution. Symmetry-breaking transitions are usually classified into first- or second-order. During a first-order phase transition, the system either absorbs or releases a fixed amount of energy that is called latent heat. Because energy cannot be instantaneously transferred between the system and its environment, first-order transitions are associated with mixed phase regimes with coexistence of the low- and high-temperature states. Conversely, a second-order phase transition does not have an associated latent heat. In this case, the order parameter defining the low-temperature phase changes continuously when the critical temperature T_c is crossed. Some examples of second-order phase transitions are the transition between the ferromagnetic and paramagnetic, superconducting and normal conducting, and charge density wave (CDW) formation; see e.g. Refs. [4, 27] for further reading.

In the following paragraphs, we will consider the case of a CDW transition and elucidate the role of electron–phonon coupling in such an instability. These transitions break the symmetry of the lattice and generally occur in low dimensional materials. The reduction of phase space from three dimensions to two or even one dimension has several important consequences. In the vicinity of the respective critical temperature, where the transition occurs, interaction effects and fluctuations are essential. As depicted in Figure 1.8a,b the Fermi surface of a one-dimensional electron gas consists of two parallel sheets that are at a distance of twice the Fermi wavevector apart (namely, $2k_F$). This peculiar topology of the Fermi surface leads to a response to an external perturbation that is dramatically different from that in higher dimensions. In particular, the charge susceptibility at zero temperature diverges at

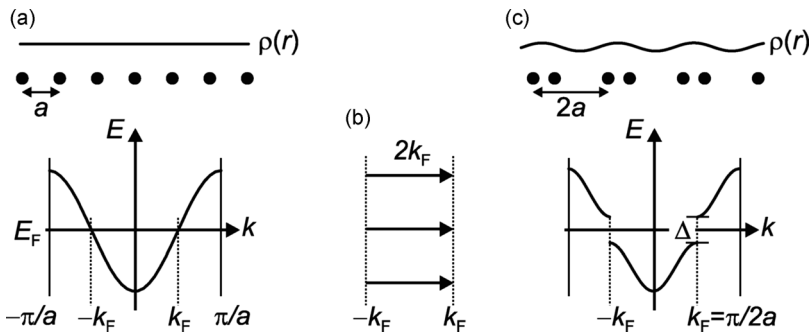


Figure 1.8 Illustration of charge density wave formation: (a) shows a half-filled band expected for a linear chain of atoms with lattice constant a for the situation of considerable wave function overlap of neighboring electrons. The first Brillouin zone extends up to $\pm\pi/a$ and the charge density $\rho(r)$ is constant. The Fermi surface of a linear chain consists of lines at $\pm k_F$ perpendicular to the line extension in real space (b). This state is highly susceptible to excitations with momenta $2k_F$, which nest

the two parts of the Fermi surface.

Corresponding rearrangement of atoms leading to a lattice constant $2a$ reduces the first Brillouin zone to $\pi/2a$, which is identical to k_F . The band gap Δ that opens as a consequence of rearrangement of ion cores turns the linear chain to an insulator. Simultaneously, $\rho(r)$ is corrugated with a periodicity of $2a$. Such a situation in low dimensional materials is referred to as a charge density wave. See Ref. [27] for more details.

wave vector $2k_F$ [27], thus implying that any infinitesimal external perturbation leads to a macroscopic charge redistribution. This phase transition leads to a modulation of the charge density with $2k_F$ periodicity in the direction perpendicular to the Fermi surface sheets. Since the CDW formation comes along with the distortion of the lattice, the transition costs elastic energy. However, the development of the $2k_F$ periodicity creates an energy gap that removes the Fermi surface, which is illustrated in Figure 1.8c. As a consequence, the energy lowering of electronic states compensates the elastic energy that is necessary for the distortion. In this case, the materials become insulating because of the vanishing carrier density associated with formation of the CDW periodicity. If the Fermi surface is not completely degenerate with respect to a $2k_F$ translation, the so-called “nesting condition” is not perfect. In this case, the Fermi surface is only partially removed and the compound remains metallic down to low temperature. A typical family of CDW materials with imperfect nesting comprehends the rare earth tellurides $R\text{Te}_3$ (with $R = \text{La}, \text{Ce}, \text{Y}, \dots$). Figure 1.9 shows the Fermi surface of CeTe_3 in the low-temperature CDW phase [30]. Notice that part of the spectral intensity on the Fermi surface is removed by the coherent scattering associated with the CDW periodicity. Even if the long-range order of the CDW vanishes above a temperature T_c , the low dimensional fluctuations of the density wave potential persist over a much broader temperature range. As a consequence, the charge gap of the CDW phase evolves in a pseudogap phase above T_c . An approximate theory accounting for the strong effects of fluctuations on the electronic excitation has been developed by Lee *et al.* [31].

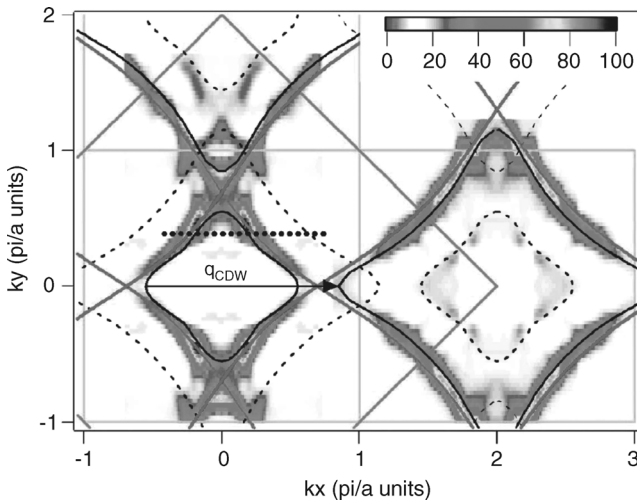


Figure 1.9 Fermi surface of CeTe_3 obtained by ARPES at the temperature of 25 K. In the horizontal direction, the Fermi surface is gapped due to charge density wave formation along this direction due to Fermi surface nesting

with a momentum q_{CDW} ; reprinted with permission from Ref. [30]. Copyright (2004) by the American Physical Society. (Please find a color version of this figure on the color plates.)

Like the electrons, the lattice excitations also display anomalies that are related to the charge density wave. Notably, the quantum energy of the phonon mode that is responsible for the Fermi surface nesting exhibits a strong temperature dependence. The lowering of quantum energy in the CDW phase is also known as a Kohn anomaly and explains the occurrence of a static lattice distortion.

In the context of the present book, we note that the excitation of such a “soft phonon” by a femtosecond optical perturbation can directly modify the amplitude of the charge density wave. Due to the impulsive character of the photoexcitation, the coherent oscillations of CDW amplitude modulate the electronic states in the gapped region of the Fermi surface. Recent time-dependent angle-resolved photoelectron spectroscopy (ARPES) experiments showed that the perturbation of the CDW turns out to be highly enhanced in the region of reciprocal space where the nesting is optimal [32]. It follows that optical perturbation is a promising tool for the exploration of charge ordering in highly correlated materials. In particular, short-range ordered patterns with checkerboard structure have been detected in several high-temperature superconductors. It is still an open question whether such charge-ordered phases are related to the electronic pseudogap of the cuprates.

1.4.5

Cooperation Between Lattice Instabilities and Electronic Correlations: The Example of Vanadium Dioxide

We end this chapter with a discussion of another exemplary material that is vanadium dioxide (VO_2). It has triggered much interest over decades due to its metal–insulator transition as a function of temperature [33]. It is metallic in its high-temperature phase of rutile structure and cooling beneath 340 K provokes a phase transition to a monoclinic insulating phase. The nature of this transition – Peierls or Mott – has been the subject of a long-standing debate. For a review, see, for example, Ref. [34]. Recent work can be found, for example, in Ref. [35–37].

The metal–insulator transition in VO_2 is accompanied by a doubling of the unit cell due to the dimerization of vanadium atoms and tilting of VO octahedra with respect to the crystallographic c -axis. According to early considerations by Goodenough, this dimerization leads to a bonding–antibonding splitting of the half-filled a_{1g} orbital, responsible for hopping along that axis, and a subsequent opening of the insulating gap between the bonding a_{1g} band and the conduction e_g^* states. This picture suggests that the gap opening in the monoclinic phase could be described within a simple band scenario, resulting from the Peierls distortion. Nevertheless, band structure calculations within density functional theory in the local density approximation result in metallic Kohn–Sham densities of states for both the rutile and the monoclinic phase. It is only when the dimerization is artificially exaggerated [34] that the Kohn–Sham band structure exhibits a gap.

Vanadium dioxide has served as an example for a compound where correlation effects are important for inducing the insulating state in the early work by Sir Neville Mott. This view was supported by experimental findings by Pouget *et al.*, who

investigated mixed phases of VO_2 under uniaxial pressure or Cr doping. These phases could, in fact, be classified as Mott insulators on the basis of their magnetic response. In the pure monoclinic phase, the magnetic susceptibility is constant and of low value, indicating the formation of a singlet state in the bonding a_{1g} band of the V-dimers.

Dynamical mean field calculations allowed to resolve the apparent contradictions outlined above shown results for the local spectral function [38–40] agree well with experimental findings as provided by (angle-integrated) photoemission and X-ray absorption spectra. In particular, the characteristic features of the metal, with a pronounced peak at the Fermi level, and a lower Hubbard satellite have been experimentally confirmed [41]. Besides one-particle spectra, the optical conductivity of experiments and LDA + DMFT calculations are in agreement [42].

Particularly interesting is the debate on the band versus Mott mechanism [37] where LDA + DMFT obtains the insulating nature of the monoclinic phase as a consequence of subtle changes in the electronic structure due to the dimerization (giving rise to pronounced bonding–antibonding splitting in the a_{1g} states) and correlations enhancing both the orbital polarization and the bonding–antibonding splitting. The resulting state was thus described as a “correlation-assisted Peierls insulator.” It was moreover shown (see Figure 1.10) that starting from the full LDA + DMFT solution, an effective static, albeit orbital-dependent, potential can be constructed that reproduces the full k -dependent spectral function. It would be too simple, however, to conclude from the existence of such an effective band structure for the insulating phase of VO_2 on *weak* correlation effects in this compound in general. This is already clear from an analysis of the *metallic* phase, which displays clear correlated features. From transport experiments, it was inferred that rutile VO_2

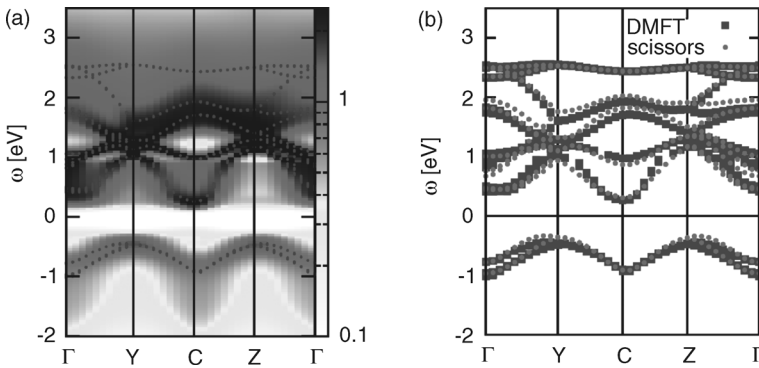


Figure 1.10 Spectral function of the insulating phase of vanadium dioxide, as calculated from LDA + DMFT. The origin of energy has been chosen as the Fermi level. (a) The maxima of the spectral function follow closely the poles of the one-particle spectral function (blue dots), stressing that sharply defined one-particle excitations exist in this phase. (b) Starting from

the full LDA + DMFT solution, a static orbital-dependent potential has been constructed. The band structure corresponding to this potential is plotted in red dots and compared with the DMFT result of (a); reprinted with permission from Ref. [37]. Copyright (2008) by the American Physical Society. (Please find a color version of this figure on the color plates.)

might be a “bad metal” in the sense that the Ioffe–Regel–Mott resistivity limit is surpassed [43]. Photoemission spectroscopy identifies a lower Hubbard band, and the DMFT calculations interpret the broad features as manifestations of very poorly defined band states, due to lifetime effects. This is also supported by the proximity to the Mott insulating mixed phases obtained under Cr doping. From a fundamental physics point of view, this coexistence of an insulating phase, whose spectral function is well described by an effective band structure (even if beyond LDA and – due to the orbital-dependence of the effective potential – even beyond DFT), and strongly correlated metallic and Mott insulating phases in the same compound is particularly intriguing.

Several time-resolved experiments provided insight into the structural deformation and the optical response of VO₂ upon a photoinduced transition. The absorption of a near-IR photon removes an electron from the bonding orbital, destabilizing the dimer and launching a coherent structural deformation that oscillates with frequency of 6 THz around the new potential minimum. The atomic motion has been imaged by X-ray diffraction [44], by X-ray absorption [45], or by means of electron diffraction [46]. The authors observed two types of dynamics, indicating a stepwise atomic motion along different directions. It has been concluded that the initial fs motion is along *a*-axis, which is the direction of the V–V bond in the monoclinic structure. On the other hand, a subsequent and slower structural transformation projects along the *c*- and *b*-axes. The optical response does follow the fast dynamics of the Vanadium dimerization, namely, on a timescale of 75 fs. The authors conclude that the coherently initiated structural motion, brought about by optical phonons, is the most likely explanation for the collapse of the band gap [47]. Further experimental evidence for such behavior has been brought about by time-resolved THz experiments on thin films [48].

References

- 1 Drude, P. (1900) *Ann. Phys.*, **1**, 535.
- 2 Smith, N.V. (1970) *Phys. Rev. B*, **2**, 2840.
- 3 Ashcroft, N.W. and Mermin, N.D. (1976) *Solid State Physics*, Hartcourt College Publishers.
- 4 Jensen, E. and Plummer, E.W. (1985) *Phys. Rev. Lett.*, **55**, 1912.
- 5 Perdew, J.P. and Levy, M. (1983) *Phys. Rev. Lett.*, **51** 1884.
- 6 Mott, N.F. (1949) *Proc. Phys. Soc. Lond.*, **62**, 416.
- 7 Verwey, E.J.W. (1939) *Nature*, **144**, 327.
- 8 Imada, M., Fujimori, A., and Tokura, Y. (1998) *Rev. Mod. Phys.*, **70**, 1039.
- 9 Davis, L.C. (1982) *Phys. Rev. B*, **25**, 2912.
- 10 Zaanen, J., Sawatzky, G.A., and Allen, J.W. (1985) *Phys. Rev. Lett.*, **55**, 418.
- 11 McWhan, D.B., Remeika, J.P., Rice, T.M., Brinkman, W.F., Maita, J.P., and Menth, A. (1971) *Phys. Rev. Lett.*, **27**, 941.
- 12 Poteryaev, A.I., Tomczak, J.M., Biermann, S., Georges, A., Lichtenstein, A.I., Rubtsov, A.N., Saha-Dasgupta, T., and Andersen, O.K. (2007) *Phys. Rev. B*, **76**, 085127.
- 13 Perfetti, L., Georges, A., Florens, S., Biermann, S., Mitrovic, S., Berger, H., Tomm, Y., Höchst, H., and Grioni, M. (2003) *Phys. Rev. Lett.*, **90**, 166401.

- 14 Carter, S.A., Rosenbaum, T.F., Metcalf, P., Honig, J.M., and Spalek, J. (1993) *Phys. Rev. B*, **48**, 16841.
- 15 Okimoto, Y., Katsufuji, T., Okada, Y., Arima, T., and Tokura, Y. (1995) *Phys. Rev. B*, **51**, 9581.
- 16 Perfetti, L., Loukakos, P.A., Lisowski, M., Bovensiepen, U., Wolf, M., Berger, H., Biermann, S., and Georges, A. (2008) *New J. Phys.*, **10**, 053019.
- 17 Hubbard, J. (1963) *Proc. Roy. Soc. A*, **276**, 238.
- 18 Anderson, P.W. (1961) *Phys. Rev.*, **124**, 41.
- 19 Lichtenstein, A.I. and Katsnelson, M.I. (1998) *Phys. Rev. B*, **57**, 6884.
- 20 Anisimov, V.I., Poteryaev, A.I., Korotin, M.A., Anokhin, A.O., and Kotliar, G. (1997) *J. Phys. Condens. Matter*, **9**, 7359.
- 21 Lechermann, F., Georges, A., Poteryaev, A., Biermann, S., Posternak, M., Yamasaki, A., and Andersen, O.K. (2006) *Phys. Rev. B*, **74**, 125120.
- 22 Savrasov, S.Y., Kotliar, G., and Abrahams, E. (2001) *Nature*, **410**, 793.
- 23 Minár, J., Chioncel, L., Perlov, A., Ebert, H., Katsnelson, M.I., and Lichtenstein, A.I. (2005) *Phys. Rev. B*, **72**, 045125.
- 24 Purovskii, L., Amadon, B., Biermann, S., and Georges, A. (2007) *Phys. Rev. B*, **76**, 235101.
- 25 Savrasov, S.Y. and Kotliar, G. (2004) *Phys. Rev. B*, **69**, 245101.
- 26 Pavarini, E., Biermann, S., Poteryaev, A., Lichtenstein, A.I., Georges, A., and Andersen, O.K. (2004) *Phys. Rev. Lett.*, **92**, 176403.
- 27 Grüner, G. (2000) *Density Waves in Solids, Frontiers in Physics*, Vol. 89, Perseus Publishing, Cambridge, MA, USA.
- 28 Landau, L.D. (1957) *Sov. Phys. JETP*, **3**, 920.
- 29 Landau, L.D. (1957) *Sov. Phys. JETP*, **5**, 101.
- 30 Brouet, V., Yang, W.L., Zhou, X.J., Hussain, Z., Ru, N., Shin, K.Y., Fisher, I.R., and Shen, Z.-X. (2004) *Phys. Rev. Lett.*, **93**, 126405.
- 31 Lee, P.A., Rice, T.M., and Anderson, P.W. (1973) *Phys. Rev. Lett.*, **31**, 462.
- 32 Schmitt, F., Kirchmann, P.S., Bovensiepen, U., Moore, R.G., Rettig, L., Krenz, M., Chu, J.-H., Ru, N., Perfetti, L., Lu, D.H., Wolf, M., Fisher, I.R., and Shen, Z.-X. (2008) *Science*, **321**, 1649.
- 33 Morin, F.J. (1959) *Phys. Rev. Lett.*, **3**, 34.
- 34 Eyert, V. (2002) *Ann. Phys.*, **11** (9), 650.
- 35 Tanaka, A. (2006) *Phys. Rev. B*, **378–80**, 269–270.
- 36 Tomczak, J.M. and Biermann, S. (2007) *J. Phys. Condens. Matter*, **19**, 365206.
- 37 Tomczak, J.M., Aryasetiawan, F., and Biermann, S. (2008) *Phys. Rev. B*, **78**, 115103.
- 38 Laad, M.S., Craco, L., and Müller-Hartmann, E. (2006) *Phys. Rev. B*, **73**, 195120.
- 39 Liebsch, A., Ishida, H., and Bihlmayer, G. (2005) *Phys. Rev. B*, **71**, 085109.
- 40 Biermann, S., Poteryaev, A., Lichtenstein, A.I., and Georges, A. (2005) *Phys. Rev. Lett.*, **94**, 026404.
- 41 Koethe, T.C., Hu, Z., Haverkort, M.W., Schüßler-Langeheine, C., Venturini, F., Brookes, N.B., Tjernberg, O., Reichelt, W., Hsieh, H.H., Lin, H.-J., Chen, C.T., and Tjeng, L.H. (2006) *Phys. Rev. Lett.*, **97**, 116402.
- 42 Tomczak, J.M. and Biermann, S. (2009) *Phys. Rev. B*, **80**, 085117; Tomczak, J.M. and Biermann, S. (2009) *Europhys. Lett.*, **86**, 37004; Tomczak, J.M. and Biermann, S. (2009) *Phys. Stat. Sol. B*, **246**, 9.
- 43 Qazilbash, M.M., Brehm, M., Andreev, G.O., Frenzel, A., Ho, P.-C., Chae, B.-G., Kim, B.-J., Yun, S.J., Kim, H.-T., Balatsky, A.V., Shpyrko, O.G., Maple, M.B., Keilmann, F., and Basov, D.N. (2009) *Phys. Rev. B*, **79**, 075107.
- 44 Cavalleri, A., Tóth, Cs., Siders, C.W., Squier, J.A., Ráksi, F., Forget, P., and Kieffer, J.C. (2001) *Phys. Rev. Lett.*, **87**, 237401.
- 45 Cavalleri, A., Rini, M., Chong, H.H.W., Fourmaux, S., Glover, T.E., Heimann, P.A., Kieffer, J.C., and

- Schoenlein, R.W. (2005) *Phys. Rev. Lett.*, **95**, 067405.
- 46 Baum, P., Yang, D.-S., and Zewail, A.H. (2007) *Science*, **318**, 788.
- 47 Cavalleri, A., Rini, M., Chong, H.H.W., Fourmaux, S., Glover, T.E., Heimann, P.A., Kieffer, J.C., and Schoenlein, R.W. (2004) *Phys. Rev. B*, **70**, 161102.
- 48 Kübler, C., Ehrke, H., Huber, R., Lopez, R., Halabica, A., Haglund, R.F., Jr., and Leitenstorfer, A. (2007) *Phys. Rev. Lett.*, **99**, 116401.

